Coherent vortex structures in quantum turbulence

2012 EPL 98 26002

(http://iopscience.iop.org/0295-5075/98/2/26002)

A Letters Journal Exploring the Frontiers of Physics

April 2012

EPL, **98** (2012) 26002
doi: 10.1209/0295-5075/98/26002

www.epljournal.org

Coherent vortex structures in quantum turbulence

A. W. Baggaley[1], C. F. Barenghi[1(a)], A. Shukurov[1] and Y. A. Sergeev[2]

[1] *School of Mathematics and Statistics, Newcastle University - Newcastle upon Tyne NE1 7RU, UK, EU*
[2] *School of Mechanical and Systems Engineering, Newcastle University - Newcastle upon Tyne NE1 7RU, UK, EU*

received 12 January 2012; accepted in final form 28 March 2012
published online 30 April 2012

PACS 67.25.dk – ^{4}He: Vortices and turbulence
PACS 47.37.+q – Hydrodynamic aspects of superfluidity; quantum fluids
PACS 47.27.De – Turbulent flows: Coherent structures

Abstract – Quantum turbulence, easily generated in superfluid helium, consists of a disordered tangle of thin, discrete vortex lines of quantised circulation which move in a fluid without viscosity. In this report we show that, in very intense quantum turbulence, the vortex tangle contains small coherent vortical structures (bundles of quantised vortices) which arise from the fundamental Biot-Savart interaction between vortices, and which are similar to the intermittent, coherent structures ("worms") observed in ordinary viscous turbulence. Our result highlights the similarity between quantum turbulence and ordinary turbulence, and sheds new light into the origin of the "worms" in ordinary turbulence.

Introduction. – It has been known since the 1980s that homogeneous isotropic turbulence contains intermittent, worm-like regions of concentrated vorticity [1–5]. Their origin is often attributed to the roll-up of vortex sheets by the Kelvin-Helmholtz instability [6,7]. Their role in the dynamics of turbulence is not clear [8]: there is no consensus as to whether they are responsible for the main properties of turbulence (for example, the Kolmogorov energy spectrum) or only affect secondary features (for example, the tails of statistical distributions and the exponents of high-order structure functions).

Turbulence is also studied at temperatures near absolute zero in both isotopes (^{4}He and ^{3}He-B) of superfluid helium [9–13]. Here the viscosity is zero, the velocity field $\mathbf{v}$ is proportional to the gradient of the quantum mechanical wave function Ψ, and vorticity is constrained to one-dimensional line singularities at which the real and the imaginary parts of Ψ vanish simultaneously. The key property of these quantum fluids is that the circulation integral $\oint_{\mathcal{C}} \mathbf{v}\cdot\mathbf{dr}$ is either zero if the path $\mathcal{C}$ does not enclose a line singularity, or is equal to the quantum of circulation $\kappa = h/m$ if it does; here h is Planck's constant and m is the mass of the relevant boson (one atom for bosonic ^{4}He, or two atoms to form a Cooper pair for fermionic ^{3}He-B). The hollow, vortex core region where the condensate density (proportional to $|\Psi|^2$) drops from its bulk value to zero is very small: the vortex core radius a_0 is approximately 0.1 nm in ^{4}He and 10 nm in ^{3}He-B. The fact that the vorticity can only assume the form of thin, discrete vortex lines of fixed core radius and circulation is in sharp contrast to vortices in ordinary fluids, which are viscous, have any arbitrary size and strength, and decay due to viscous diffusion. Turbulence in superfluid helium consists of a tangle of such quantised vortices, and can easily be created in the laboratory by stirring the liquid helium. Experiments show that this "quantum turbulence" shares important properties with ordinary (classical) turbulence [10,14,15], from the drag force [16] to the Kolmogorov energy spectrum [17,18].

In this report we show that, in intense quantum turbulence, quantised vortices tend to bundle together and form coherent structures, similar to the "worms" of ordinary turbulence. Since there are no vortex sheets in superfluid helium (only vortex lines are possible), our result not only highlights a remarkable similarity between quantum turbulence and ordinary turbulence, but also questions the traditional Kelvin-Helmoltz explanation of the origin of the "worms" in ordinary turbulence.

Method. – Since the superfluid vortex core radius a_0 is orders of magnitude smaller than the typical distance between vortex lines in turbulence experiments, $\ell \approx 10^{-3}$ to 10^{-6} m, we follow the approach of Schwarz [19] and describe vortex lines as space curves $\mathbf{s}(\xi, t)$ of infinitesimal thickness, where t is time and ξ is arclength. To model quantum turbulence in its simplest form, we consider ^{4}He

(a) E-mail: c.f.barenghi@ncl.ac.uk

at temperatures below 0.7 K, so that thermal excitations are negligible and the governing equation of motion [9] reduces to the Biot-Savart law

$$\frac{\mathrm{d}\mathbf{s}}{\mathrm{d}t} = -\frac{\kappa}{4\pi}\oint_{\mathcal{L}} \frac{(\mathbf{s}-\mathbf{r})}{|\mathbf{s}-\mathbf{r}|^3} \times \mathbf{dr}, \tag{1}$$

where $\kappa = 10^{-7}\,\mathrm{m}^2/s$ in ^{4}He, and the line integral extends over the entire vortex configuration $\mathcal{L}$. Equation (1) expresses Euler dynamics in integral form [20]. However, unlike classical Euler vortices, quantised vortices reconnect if they come very close to each other, as demonstrated using the Gross-Pitaevskii equation (GPE) for the Bose-Einstein condensate [21] and seen directly in recent experiments [22]. To account for this effect, again following Schwarz [19], the Biot-Savart law is complemented by an algorithmic reconnection procedure.

The numerical techniques to discretise the vortex lines, regularise the Biot-Savart integrals, compute them with a tree algorithm, time step the vortex lines and perform reconnections are described in the literature [19,23] and in our previous papers [24–26]. Our numerical algorithm which controls the discretization enforces the given separation $\Delta\xi$ between points on the vortex line to remain between 2×10^{-6} m and 4×10^{-6} m during the evolution. We have tested that our result does not depend on the numerical resolution.

Our vortex reconnection procedure [27] guarantees that a small amount of vortex length (as a proxy for kinetic energy) is lost at each reconnection, in agreement with numerical calculations of vortex reconnections performed using the GPE [28]. The reconnection procedure and the enforcement of the minimum distance $\Delta\xi$ provide the numerical dissipation mechanism which plays the rôle of phonon emission in ^{4}He [10,24] or of the Caroli-Matricon [29] mechanism in ^{3}He-B.

It must be stressed that, unlike classical vortex methods [30–32], Schwarz's model allows neither intensification of vorticity by vortex stretching nor core diffusion: the values of the circulation κ around a vortex line and of the vortex core radius a_0 are fixed by the value of Planck's constant.

Quantum turbulence. – The first step of our numerical experiment consists in creating a sample of homogeneous isotropic quantum turbulence at zero temperature. The computational domain is a cubic periodic box of size $D = 7.5\times10^{-3}$ m. The initial condition, shown in fig. 1, consists of randomly oriented, randomly located straight vortex lines, each carrying one quantum of circulation κ; in this way we enforce isotropy and enough energy at the large lengthscales. We found that the results described below do not depend on the detailed choice of initial condition which lead to the Kolmogorov spectrum.

During the time evolution of the vortex configuration, we monitor various quantities, such as the total length Λ and the isotropy of the vortices, the vortex reconnection rate, the minimum, maximum and average values of the curvature ($C(\xi) = |\mathrm{d}^2\mathbf{s}/\mathrm{d}\xi^2|$ being the local curvature), the total energy E and the energy spectrum $E(k)$.

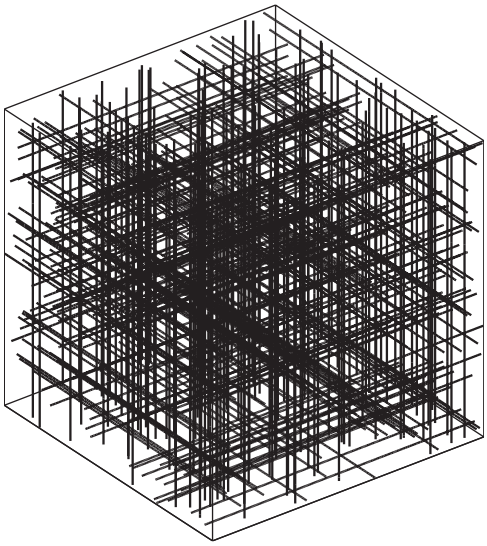

Fig. 1: Initial vortex configuration at $t = 0$ s.

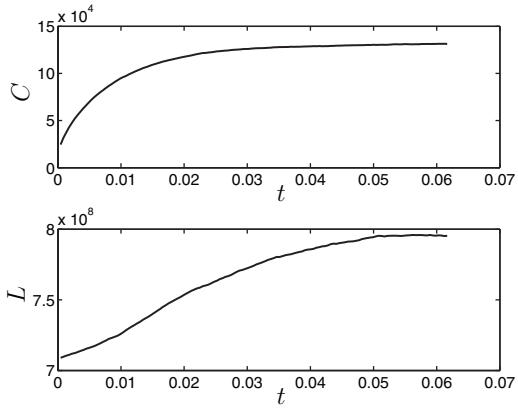

Fig. 2: Time evolution of the average curvature C, m^{-1} (top) and of the vortex line density L, m^{-2} (bottom) *vs.* time t, s.

We find that, after a transient, the vortex configuration saturates to a statistical steady state which is independent of the details of the initial conditions, in agreement with similar calculations in the literature. The evolution of the average curvature C and of the vortex line density $L = \Lambda/D^3$ (vortex length per unit volume), from the initial time $t = 0$ to the final time $t = T = 0.06$ s when we stop the calculation, are shown in fig. 2. Note that T is much greater than the turnover time τ of vortex lines around each other, which can be estimated to be of the order of $\tau \approx \ell^2/\kappa$ because the superfluid velocity at distance r from a vortex is $\kappa/(2\pi r)$. Note also that, over the time scale T, the total energy is essentially constant; the dissipative effects described in the previous section become significant only at longer time scales, causing a decay of energy and length. A snapshot of the dense vortex tangle which we obtain is shown in fig. 3. From the vortex line density,

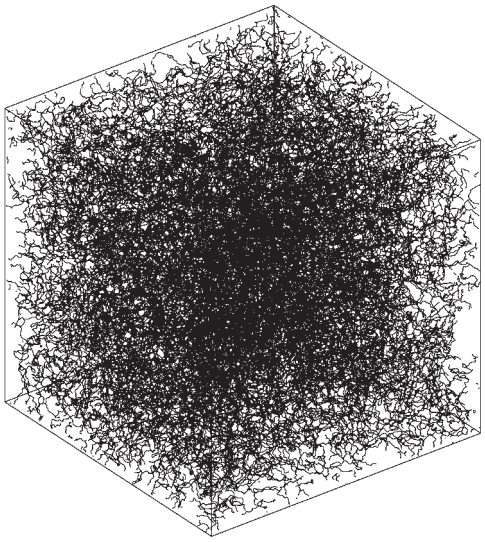

Fig. 3: Vortex tangle at $t = 0.06\,\mathrm{s}$.

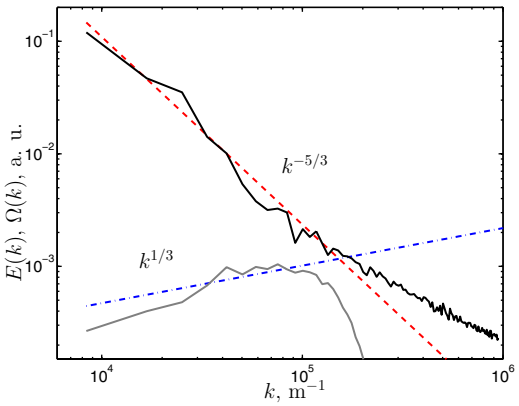

Fig. 4: (Colour on-line) Energy spectrum $E(k)$ (black line) and effective enstrophy spectrum $\Omega(k)$ (grey line), arbitrary units, *vs.* wave number k, m^{-1}. The straight dashed lines represent the classical energy $k^{-5/3}$ (red dashed line) and enstrophy $k^{1/3}$ (blue dash-dotted line) scalings.

$L = 7.9 \times 10^8\,\mathrm{m}^{-2}$, we infer that the average distance between vortex lines is approximately $\ell \approx L^{-1/2} = 0.36 \times 10^{-4}$m.

The kinetic energy spectrum $E(k)$ is defined by

$$E = \frac{1}{V}\int \frac{1}{2}\mathbf{v}^2 \mathrm{d}V = \int_0^\infty E(k)\mathrm{d}k, \qquad (2)$$

where k is the magnitude of the three-dimensional wave vector and $V = D^3$. To compute the energy spectrum we calculate the superfluid velocity $\mathbf{v}$ on a 1024^2 mesh in the xy-plane at $z = 0$, using the Biot-Savart integral, eq. (1). We verify (see fig. 4) that, at large scales $k < k_\ell = 2\pi/\ell \approx 1.8 \times 10^5\mathrm{m}^{-1}$, $E(k)$ is consistent with the $k^{-5/3}$ Kolmogorov scaling which is observed in ordinary turbulence; this result is in agreement with experiments [17,18], and with calculations performed with Schwarz's model [23,25] and the GPE [33–35].

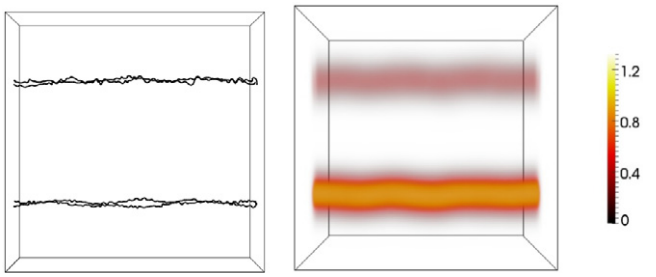

Fig. 5: (Colour on-line) Volume rendering (a semi-transparent representation) of the magnitude of the smoothed vorticity, $|\omega(\mathbf{r})|$, s^{-1}, for anti-parallel (left) and parallel (right) vortex pairs. In the former, the average vorticity is small but not zero due to the presence of small-amplitude Kelvin waves (note the wiggliness of the vortex filaments). In the latter, the contributions of the two vortex strands add up.

Coherent vortex structures. – The question which we address is whether the dense vortex tangle shown in fig. 3 contains regions of concentrated vorticity, similar to the "worms" of ordinary turbulence. Visual inspection suggests that the vortex tangle is somewhat intermittent in space. To properly answer the question, we convolve our discrete vortex filaments with a Gaussian kernel, and define a smoothed vorticity field $\boldsymbol{\omega}$,

$$\boldsymbol{\omega}(\mathbf{r},\, t) = \kappa \sum_{i=1}^{N} \frac{\mathbf{s}_i'}{(2\pi\sigma^2)^{3/2}} \exp(-|\mathbf{s}_i - \mathbf{r}|^2/2\sigma^2)\Delta\xi\,, \qquad (3)$$

where $\mathbf{s}_i' = \mathrm{d}\mathbf{s}_i/\mathrm{d}\xi$ is the unit vector along a vortex at $\mathbf{s}_i = \mathbf{s}_i(\xi, t)$, and the smoothing length σ is of the order of ℓ; N is the number of discretization points. We test that, under this smoothing operation, a collection of randomly oriented vortex lines whose separation is of the order of ℓ yields $\boldsymbol{\omega} \approx \mathbf{0}$; conversely, an organised bundle of vortex filaments of the same circulation yields a smooth vorticity distribution. We also take into account the fact that, in the absence of mutual frictionv [36] in the low temperature limit, our calculation is in the presence of a Kelvin waves cascade [24] for $k > k_\ell$, hence the vortex lines are very wiggly. Figure 5 tests the smoothed vorticity resulting from adding ten helical waves with an imposed $k^{-7/5}$ Kelvin wave amplitude spectrum.

From the smoothed vorticity ω we can define an effective enstrophy spectrum $\Omega(k)$. We find that it is consistent with the classical $k^{1/3}$ scaling, peaking near $k \approx k_\ell$ as expected, see fig. 4.

Figure 6 shows the smoothed vorticity corresponding to fig. 3: vortical "worms", such as those seen in numerical simulations of ordinary turbulence, are clearly visible. Each "worm" consists of parallel vortex lines which, in a small region of space, are close to each other, creating a relatively large $\boldsymbol{\omega}$, and then fan away from each other outside this region where $\boldsymbol{\omega}$ is much smaller due to the random orientation of the lines.

There have been reports in the literature about the existence of vortex bundles [37,38] in simulations of

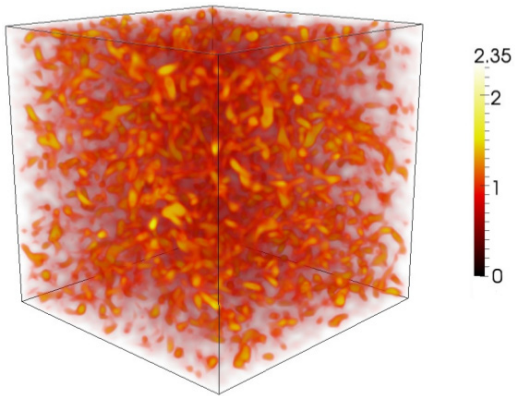

Fig. 6: (Colour on-line) Volume rendering of $|\boldsymbol{\omega}(\mathbf{r})|$, s^{-1} corresponding to fig. 3. Note the vortical worm-like structures, similar to the "worms" observed in ordinary turbulence.

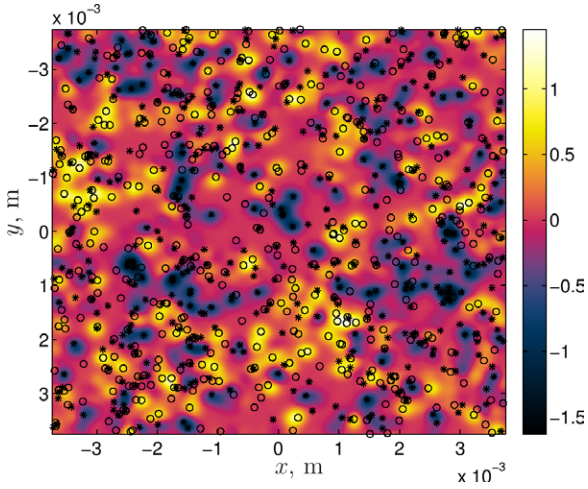

Fig. 7: (Colour on-line) Cross-section $z=0$ of $\omega_z(\mathbf{r}), \mathrm{s}^{-1}$ from fig. 6. Open circles show where vortex lines cross the plane from $z<0$, and black asterisks show those coming from $z>0$. Clustering of vortex points of the same sign is visible as regions of large positive and negative values of ω_z (shown blue and yellow).

quantum turbulence at relatively high temperatures, $0.7\,\mathrm{K} < T < T_\lambda \approx 2.17\,\mathrm{K}$, where thermal excitations form a viscous normal fluid component which interacts with the vortex lines via a friction force. However, in this finite-temperature regime, vortical structures belong to the normal turbulent fluid, and the friction force [39] would naturally induce superfluid bundles around them (although their stability is an open question). What we have shown in this report is the development of vortical bundles in the perfect superfluid case, as a consequence of pure Euler dynamics. A visually intermittent vortex structure has also been noticed in a recent [40] GPE simulation of turbulence in a Bose-Einstein condensate. However, in this work the vortex cores were very close to each other: $\ell/a_0 \approx 4.5$ to 9 (in contrast to our much larger $\ell/a_0 \approx 3.5\times10^3$ typical of helium experiments): compressible effects (rapid density changes near vortex cores, sound waves, and the application of artificial damping, which affects vortex positions) were likely to have played a rôle.

Analysis of the coherent structures. – To verify that the worm-like structures in fig. 6 are indeed bundles of quantised vortices, we show in fig. 7 a two-dimensional cross-section of the z-component of the smoothed vorticity $\boldsymbol{\omega}$ in the $z=0$ plane of fig. 6. We overlay the intersections of vortex filaments with the plane $z=0$ distinguishing the sign of ω_z. It is apparent that the smoothed vortical structures shown in fig. 6 are indeed small bundles of aligned vortex filaments, which appear as small clusters of positive and negative vorticity. There are typically 2 to 5 vortex points in each cluster.

It is important to check that the vortex bundles are physically distinct coherent structures of a well-defined scale, rather than just a part of a purely random distribution, which would also contain structures of any scale which would become prominent after averaging. Clustering in any two-dimensional system of points (or of any other discrete objects) can be confirmed and quantified using Besag's function [41],

$$L(d) = \sqrt{K(d)/\pi} - d, \tag{4}$$

where

$$K(d) = \frac{D^2}{M^2}\sum_{i=1}^{M}\sum_{j=1,j\neq i}^{M} I(d_{i,j} < d) \tag{5}$$

is Ripley's K-function [42], M is the number of points within the area $A=D^2$ (D being the size of the domain), $d_{i,j}$ is the distance between points i and j, and $I(x)$ is unity if the condition x is satisfied and zero otherwise. These functions are frequently used in applied statistics to detect spatial correlations in two-dimensional systems: $L(d)=0$ means complete spatial randomness, $L(d)<0$ implies dispersion, and $L(d)>0$ aggregation (clustering). Figure 8 shows Besag's function for a large collection of two-dimensional cross-sections of the three-dimensional tangle shown in fig. 3. The figure confirms that vortex points of the same sign tend to cluster, hence the vortex clusters of fig. 7 represent indeed distinct physical entities —regions of concentrated vorticity— rather than merely an element of a purely random distribution of vorticity.

Finally, we have verified the existence of the coherent vortex structures at a lower numerical resolution ($\Delta\xi \sim 10^{-5}\,\mathrm{m}$) for approximately the same vortex line density, $L \approx 10^9\,\mathrm{m}^{-2}$. The lower resolution allows us to monitor the continual appearance and disappearance of "worms" over a longer time scale, of the order of 1 s. We find that the typical width of "worms" is approximately 2 times ℓ and the typical lifetime is of the order of 10 times the turnover time scale $\tau = \ell^2/\kappa$. We also note that the worms have a characteristic elongated structure with a typical aspect

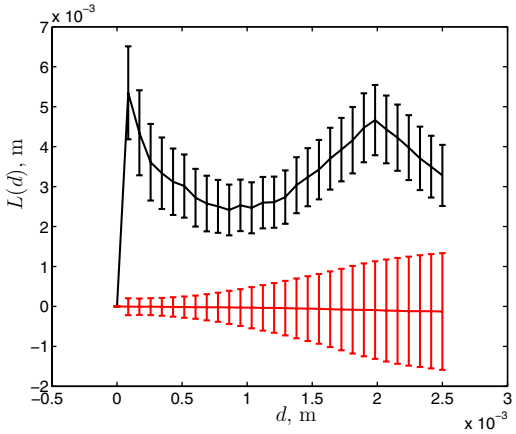

Fig. 8: (Colour on-line) Besag's function, $L(d)$, averaged over a random selection of 1000 two-dimensional cross-sections (parallel to one of the coordinate planes) of the vortex tangle of fig. 3 in the final, statistically steady state (black) and the initial state (red), plotted *vs.* distance, d. Vertical bars show one standard deviation range. The initial state has $L(d) = 0$ within errors at all scales, consistently with the purely random nature of the initial conditions. In the final state $L(d) > 0$ at all scales, confirming the existence of coherent structures (clusters of vortex filaments in each cross-section).

Fig. 9: (Colour on-line) An isolated structure from the lower-resolution simulation, $\Delta\xi \sim 10^{-5}$ m, with the vortices that make up the structure plotted as black lines, and other nearby vortices plotted in grey. We estimate the width of this structure to be approximately 2ℓ.

ratio of 5 : 1. Figure 9 shows an isolated vortical structure from the lower-resolution simulation.

Conclusions. – In conclusion, our numerical experiments with quantum turbulence at absolute zero have revealed that the vortex tangle contains coherent vortical structures, or bundles of parallel vortex lines, which arise from the Biot-Savart dynamics alone, and appear to be similar to the vorticity "worms" observed in ordinary turbulence. Unlike ordinary turbulence, in a superfluid system the vorticity is only in the form of lines, hence the vortex bundles which we observe are not the result of the Kelvin-Helmoltz roll-up of vortex sheets. The result sheds new light on the relation between ordinary and quantum turbulent flows, suggesting that their connection can be deeper than usually assumed. Given the relative simplicity of the quantum turbulence, this may provide new insights into the nature of turbulence and the origin of "worms".

* * *

We are grateful to the European Community (HPC-EUROPA2 project 228398) and to the Leverhulme Trust (grants F/00125/AH and RPG-097) for financial support, and to P. A. Davidson and Y. Kaneda for discussions.

REFERENCES

[1] Siggia E. D., *J. Fluid Mech.*, **107** (1981) 375.
[2] Kerr R. M., *J. Fluid Mech.*, **153** (1985) 31.
[3] Douady S. *et al.*, *Phys. Rev. Lett.*, **67** (1991) 983.
[4] Moffatt H. K. and Kida S., *Annu. Rev. Fluid Mech.*, **259** (1994) 241.
[5] Sreenivasan K. R. and Antonia R. A., *Annu. Rev. Fluid Mech.*, **29** (1997) 435.
[6] Vincent A. and Meneguzzi M., *J. Fluid Mech.*, **258** (1994) 245.
[7] Davidson P. A., *Turbulence* (Oxford University Press) 2004.
[8] Frisch U., *Turbulence: The Legacy of A. N. Kolmogorov* (Cambridge University Press) 1995.
[9] Donnelly R. J., *Quantized Vortices in Helium II* (Cambridge University Press) 1991.
[10] Vinen W. F. and Niemela J. J., *J. Low Temp. Phys.*, **128** (2002) 167.
[11] Walmsley P. M. and Golov A. I., *Phys. Rev. Lett.*, **100** (2008) 245301.
[12] Bradley D. I. *et al.*, *Nat. Phys.*, **7** (2011) 473.
[13] Eltsov V. B. *et al.*, *Phys. Rev. Lett.*, **99** (2007) 265301.
[14] Skrbek , *JETP Lett.*, **80** (2006) 474.
[15] L'vov V. S. *et al.*, *J. Low Temp. Phys.*, **145** (2006) 125.
[16] Smith M. R. *et al.*, *Phys. Fluids*, **11** (1999) 751.
[17] Maurer J. and Tabeling P., *Europhys. Lett.*, **43** (1998) 29.
[18] Salort J. *et al.*, *Phys. Fluids*, **22** (2010) 125102.
[19] Schwarz K. W., *Phys. Rev. B*, **38** (1988) 2398.
[20] Saffman P. G., *Vortex Dynamics* (Cambridge University Press) 1992.
[21] Koplik J. and Levine H., *Phys. Rev. Lett.*, **71** (1993) 1375.
[22] Bewley G. P. *et al.*, *Proc. Natl. Acad. Sci. U.S.A.*, **105** (2008) 13707.
[23] Araki T. *et al.*, *Phys. Rev. Lett.*, **89** (2002) 145301.
[24] Baggaley A. W. and Barenghi C. F., *Phys. Rev. B*, **83** (2011) 134509.
[25] Baggaley A. W. and Barenghi C. F., *Phys. Rev. B*, **84** (2011) 020504.

[26] Baggaley A. W. and Barenghi C. F., *J. Low Temp. Phys.*, **166** (2012) 3.
[27] Baggaley A. W., arXiv:1109.4409 (2011), to be published in *J. Low Temp. Phys.* (2012).
[28] Leadbeater M. *et al.*, *Phys. Rev. Lett.*, **86** (2001) 1410.
[29] Kopnin N. B. *et al.*, *Europhys. Lett.*, **32** (1995) 651.
[30] Cottet G. H. *et al.*, *J. Comput. Phys.*, **175** (2002) 1.
[31] Cottet G. H. and Koumoutsakos P. D., *Vortex Methods: Theory and Practice* (Cambridge University Press) 2000.
[32] van Rees W. M. *et al.*, *J. Comput. Phys.*, **230** (2011) 2794.
[33] Nore C. *et al.*, *Phys. Rev. Lett.*, **78** (1997) 3896.
[34] Kobayashi M. and Tsubota M., *Phys. Rev. Lett.*, **94** (2005) 065302.
[35] Yepez Jeffrey *et al.*, *Phys. Rev. Lett.*, **103** (2009) 084501.
[36] Barenghi C. F. *et al.*, *J. Low Temp. Phys.*, **52** (1983) 189.
[37] Kivotides D., *Phys. Rev. Lett.*, **96** (2006) 175301.
[38] Morris K. *et al.*, *Phys. Rev. Lett.*, **101** (2008) 15301.
[39] Barenghi C. F. *et al.*, *Phys. Rev. Lett.*, **89** (2002) 275301.
[40] Sasa N. *et al.*, *Phys. Rev. B*, **84** (2011) 054525.
[41] Besag J. E., *J. R. Stat. Soc. B*, **39** (1977) 193.
[42] Ripley B. D., *J. Appl. Probab.*, **13** (1976) 255.